



Chemical Pre-Lithiation of LiMn_2O_4 Balances the Low First Cycle Efficiency of Silicon Anodes

Journal:	<i>Journal of Materials Chemistry A</i>
Manuscript ID	TA-COM-04-2024-002544.R1
Article Type:	Communication
Date Submitted by the Author:	24-May-2024
Complete List of Authors:	Ko, Jesse; Johns Hopkins University Applied Physics Laboratory, Tan, Bing; Johns Hopkins University Applied Physics Laboratory Logan, Matthew; Johns Hopkins University Applied Physics Laboratory, Research and Exploratory Development Department (REDD) Langevin, Spencer; Johns Hopkins University Applied Physics Laboratory Gerasopoulos, Konstantinos; Johns Hopkins University Applied Physics Laboratory, Research and Exploratory Development

ARTICLE TYPE

Cite this: DOI: 00.0000/xxxxxxxxxx

Chemical Pre-Lithiation of LiMn_2O_4 Balances the Low First Cycle Efficiency of Silicon Anodes^{†‡}

Jesse S. Ko,^{†*} Bing Tan,^{†*} Matthew W. Logan,^a Spencer A. Langevin,^a Konstantinos Gerasopoulos,^a

Received Date
Accepted Date

DOI: 00.0000/xxxxxxxxxx

Chemical pre-lithiation is carried out using lithium naphthalene to incorporate excess lithium into lithium manganese spinel (LiMn_2O_4). Pre-lithiated LiMn_2O_4 powder is collected and processed under ambient air conditions, demonstrating its seamless integration into current lithium-ion manufacturing. Precise control of the lithiation content in LiMn_2O_4 allows tuning of the first cycle efficiency, and when demonstrated in a full-cell configuration comprising a silicon anode, can achieve a projected specific energy of $\sim 216 \text{ Wh kg}^{-1}$ performance.

Energy density demands for current lithium-ion batteries necessitate novel strategies for enabling high-capacity anodes that can transition seamlessly to present lithium-ion battery manufacturing.^{1–4} Silicon (Si) has garnered immense attention over the past decade and is regarded to be the next-generation anode material to replace graphite (gr) anode.^{2–6} Si is attractive because of its high gravimetric capacity (3580 mAh g^{-1} for $\text{Li}_{15}\text{Si}_4$ at room temperature), which is nearly ten-fold higher than that of the current state-of-the-art gr (372 mAh g^{-1}).⁷ Additionally, Si is appealing because it is the second most abundant element in the Earth's crust, it is environmentally benign, and has a low electrochemical potential ($\sim 0.37 \text{ V vs. Li/Li}^+$).⁷ When paired with a cathode material, the key challenge for commercial Si-based cells is to properly balance the low initial Coulombic efficiency (ICE).

Spinel lithium manganese oxide (LiMn_2O_4 ; LMO) is a cost-effective, stable, and safe cathode material that has been incorporated into batteries used for such applications as electric buses, hybrid electric vehicles, and large-scale grid applications.^{8–10} This material is traditionally synthesized via solid-state reaction in air, and the material cost is expected to be the lowest versus all other viable cathode materials (e.g., lithium cobalt oxide, lithium nickel manganese cobalt oxide, etc.) because it is nickel- and cobalt-free. The drawback of LMO is its relatively low energy density, arising from its limited capacity (theoretical capacity: 148

mAh g^{-1});¹¹ yet, if paired with a high energy and cost-effective anode material (e.g., Si), a compelling, low-cost lithium-ion cell can be developed for next-generation storage. The ICE of LMO can be as high as 97%,¹² while Si ranges between 60 to 75%.¹³ Due to this mismatch, the full capacity of LMO cannot be utilized in a full-cell configuration, which would be detrimental to the overall energy density. This proposed Si||LMO cell is expected to have better low-temperature performance, better charging rate, higher energy density, and lower cost than the corresponding gr||LMO cell.¹⁴ We project that a Si||LMO cell with a proper balance in ICE can yield $\sim 216 \text{ Wh kg}^{-1}$ for a 20 Ah design. Lastly, this combination offers strategic advantages in terms of supply chain security, where both Si and LMO are natural abundant elements.

Matching the ICE between the cathode and anode is a critical step in maximizing active material usage.^{15,16} Recently, a few reports using pre-lithiated Si for full cells have been demonstrated;^{17–23} however, pre-lithiated Si requires an inert atmosphere since the lithiated form of this material is highly sensitive to moisture and oxygen because of their low potentials, which casts considerable doubt on their feasibility for large-scale commercialization. Conversely, only a few studies report pre-lithiated LMO paired with anode materials that exhibit relatively low ICE.^{24–26} Tarascon et al. reported that pre-lithiated LMO was stable in air using lithium iodide as the reducing reagent; yet, this process generates a highly corrosive iodine vapor, which will exacerbate safety concerns and production costs.²⁵ Moorhead-Rosenberg et al. reported a microwave reduction process carried out at $190\text{--}200 \text{ }^\circ\text{C}$ with tetraethylene glycol as the reducing agent where the ICE was measured to be $\sim 63\%$ with partially-lithiated $\text{Li}_{1.3}\text{Mn}_2\text{O}_4$.²⁶ This method is promising at the laboratory scale, but because this procedure relies on the use of microwave reactors, production at the industrial scale is not amenable. For scalability, the use of a chemical reducing agent in the solution phase presents a promising option for pre-lithiation or via roll-to-roll manufacturing via contact pre-lithiation.^{27,28} Peramunage et al. reported on the synthesis of $\text{Li}_{1+x}\text{Mn}_2\text{O}_4$ ($0 < x < 1$) with butyl lithium, which has been produced in kilogram quantities by their industrial partner.²⁹ However, butyl lithium is highly reactive and

^a Research and Exploratory Development Department, Johns Hopkins University Applied Physics Laboratory, 11100 Johns Hopkins Rd., Laurel, MD, 20723, USA; E-mail: Jesse.Ko@jhuapl.edu

[†] Authors contributed equally to this work.

[‡] Electronic Supplementary Information (ESI) available: See DOI: 00.0000/00000000.

can readily catch fire under ambient conditions. Moreover, the prepared $\text{Li}_{1+x}\text{Mn}_2\text{O}_4$ is reported to be highly hygroscopic.³⁰ As a result, it becomes necessary to discover alternative organolithium reagents that are stable in air for pre-lithiation.

As a mild reducing agent, lithium naphthalene has been reported as a safe, reducing agent with a redox potential of ~ 0.35 V vs. Li/Li^+ .^{20,27,31} The spontaneous formation of a dark blue/green solution containing lithium naphthalene due to the delocalization of the lone pair of electrons on the conjugated aromatic ring was stable in air without heat generation. Lithium naphthalene has been demonstrated successfully in improving capacity and cycle life for lithium iron phosphate and lithium nickel manganese cobalt oxide cathodes.^{32,33} In the present study, we demonstrate the use of lithium naphthalene as a scalable and stable pre-lithiation technique for LMO at room temperature. Because this pre-lithiated LMO can be processed and handled in air with high tolerance (up to 30 days) in ambient conditions, we then pair it with a Si anode to assess its advantage in improving the cell energy density by balancing the ICE of both electrode materials.

The $\text{Li}_{1+x}\text{Mn}_2\text{O}_4$ powders with varying lithium content ($0 < x < 1$) were prepared with lithium naphthalene and the compositions were expressed as the molar ratio between the added lithium and pristine LMO (**Table S1**). Briefly, lithium and LMO powder were added into a pre-dissolved solution comprising lithium naphthalene and tetrahydrofuran with the ratio of lithium to LMO being 0.35, 0.6, and 1.0, corresponding to the additional mols of lithium incorporated into LMO. The four compositions of $\text{Li}_{1+x}\text{Mn}_2\text{O}_4$ studied herein are: (i) $\text{Li}_{1.0}\text{Mn}_2\text{O}_4$ ($\text{Li}_{1.0}\text{MO}$); (ii) $\text{Li}_{1.35}\text{Mn}_2\text{O}_4$ ($\text{Li}_{1.35}\text{MO}$); (iii) $\text{Li}_{1.6}\text{Mn}_2\text{O}_4$ ($\text{Li}_{1.6}\text{MO}$); and (iv) $\text{Li}_{2.0}\text{Mn}_2\text{O}_4$ ($\text{Li}_{2.0}\text{MO}$), denoted based on the additional mols of lithium originating from the lithium naphthalene solution. X-ray diffraction and subsequent Rietveld refinement was performed to characterize the structural (and phase) evolution of the pre-lithiated LMO powders. Pristine LMO exhibits the spinel crystal framework, while overlithiation leads to the tetragonal phase of $\text{Li}_2\text{Mn}_2\text{O}_4$ (L2MO). The crystal structures of each respective phase (spinel and tetragonal) are illustrated in **Fig. S1**. For this series of pre-lithiated LMO materials, Rietveld refinements yielded goodness-of-fit factors (R_{wp}) of less than 7.5%, which provided us the confidence in quantifying the phase evolution between the spinel and tetragonal phases (**Fig. 1**). As expected, the phase for $\text{Li}_{1.0}\text{MO}$ matches that for the LMO spinel crystal structure, while $\text{Li}_{2.0}\text{MO}$ exhibits the tetragonal L2MO structure. In between, we see a distribution between these two phases, where $\text{Li}_{1.35}\text{MO}$ yields 46% and 54% of the LMO and L2MO phases, respectively. For $\text{Li}_{1.6}\text{MO}$, 22% and 78% of the LMO and L2MO phases, respectively, are present. This suggests that during the 1st charge/discharge cycle, the presence of additional mols of lithium will alter the ICE of this series of materials due to the presence of the tetragonal phase L2MO. The presence of the tetragonal L2MO spinel phase leads to additional capacity at ~ 3.0 V vs. Li/Li^+ where the occupation of Li transitions from octahedral sites (16c) to tetrahedral sites (8a), which arises from the transition to a lack of Jahn-Teller distortions in the cubic spinel LMO phase.^{34–36} During subsequent discharge down to 3.0 V vs. Li/Li^+ , the cubic

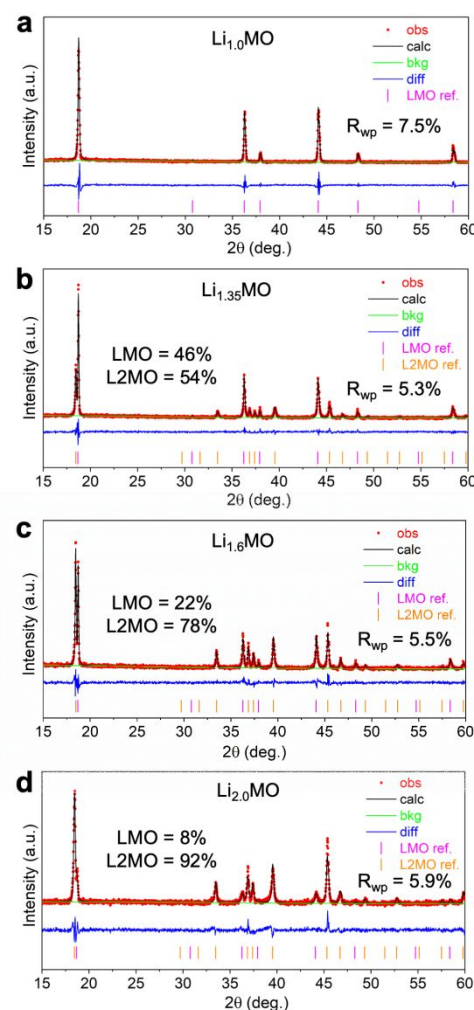


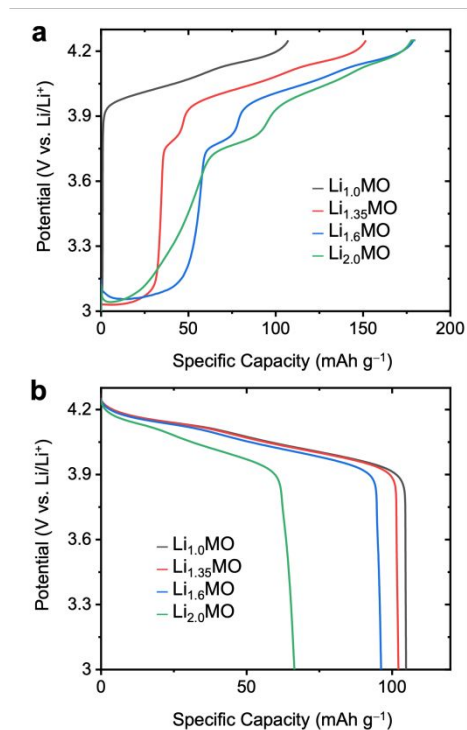
Fig. 1 Rietveld-refined X-ray diffraction patterns for this series of $\text{Li}_{1+x}\text{Mn}_2\text{O}_4$ pre-lithiated materials: (a) $\text{Li}_{1.0}\text{MO}$; (b) $\text{Li}_{1.35}\text{MO}$; (c) $\text{Li}_{1.6}\text{MO}$; and (d) $\text{Li}_{2.0}\text{MO}$. LMO refers to LiMn_2O_4 while L2MO refers to $\text{Li}_2\text{Mn}_2\text{O}_4$ crystal phases.

phase LMO will not electrochemically convert back to the tetragonal phase L2MO; thus, enabling the capability to tune ICE.

Half-cell tests employing a lithium metal as both the counter and reference were carried out to assess the specific capacities and ICE for this series of $\text{Li}_{1+x}\text{Mn}_2\text{O}_4$ materials at C/5 (**Fig. 2**). The areal mass loadings of this series of electrodes ranged between ~ 8 – 8.5 mg cm^{-2} , motivating our interest for testing under technologically-relevant conditions. For pristine $\text{Li}_{1.0}\text{MO}$, the 1st cycle efficiency was measured to be 97% (charge capacity: 108 mAh g^{-1} ; discharge capacity: 105 mAh g^{-1} ; **Table S2**), which is the expected value for LiMn_2O_4 .³⁷ With an increase in the lithium content, the ICE decreases commensurately from 97% to 43% for $\text{Li}_{2.0}\text{MO}$, all while exhibiting an increase in the 1st charge capacity up to 184 mAh g^{-1} . These values are comparable to those reported in the literature, where a microwave-assisted process was performed (63% for $x=0.3$, 54% for $x=0.65$, and 43% for $x=0.83$).¹² The changes in ICE reflect the difference in charge and discharge capacity (ΔQ), where for $\text{Li}_{2.0}\text{MO}$, the difference is

Table 1 Calculated cathode properties for Si/gr||Li_{1+x}Mn₂O₄ full cells (Li_{1.0}MO, Li_{1.35}MO, and Li_{1.6}MO).

Cathode Material	End Anode Potential at Discharge/V vs. Li/Li ⁺	Cathode Charge Capacity/mAh g ⁻¹	Cathode Discharge Capacity/mAh g ⁻¹
Li _{1.0} MO	1.04	109	63
Li _{1.35} MO	0.86	161	100
Li _{1.6} MO	0.69	186	98

Fig. 2 (a) Charge and (b) discharge profiles of this series of Li_{1.0}MO, Li_{1.35}MO, Li_{1.6}MO, and Li_{2.0}MO pre-lithiated cathode materials discharged at C/5.

nominal discharge capacity of Li_{1.0}MO; thus, demonstrating that 1.0 mol of Li is being consumed during the charge process. With the ability to tune the ICE of Li_{1+x}Mn₂O₄, we then investigated the incorporation of these electrodes with a Si anode to demonstrate the effects of pre-lithiation on full cell energy densities.

To properly pair the Li_{1+x}Mn₂O₄ electrodes, we then tested half-cells of Si/gr carbon-composite electrodes and assessed its specific capacity and ICE (Fig. S2); these values are also tabulated in Table S3. The ICE of the Si/gr anode is primarily dictated by its lithiation depth. When fully lithiated, the ICE was measured to be 75% within a potential window ranging from 0.05 V to 1.0 V vs. Li/Li⁺. To control the lithiation depth, the lower potential limit was set to 0.11 V and 0.1 V for 32 and 56% depth, respectively. As shown in Table S3, the ICE decreases when partially lithiated to 62% and 52% for 56% and 32% lithiation depth, respectively. The overall discharge capacities increased from 835 to 1455 mAh g⁻¹, ranging from 32 to 56% lithiation depth. During lithiation, the majority of the electrolyte will decompose to form a stable electrolyte interphase (SEI) layer at potentials < 0.8 V vs. Li/Li⁺. For Si/gr, the particles will expand significantly during lithiation, exposing new surfaces that induce continuous

electrolyte decomposition.^{38–41} With higher degrees of lithiation, the irreversible capacity loss (Table S3) increases due to the generation of SEI at the newly exposed surfaces, but the percentage of the capacity loss from this growth reduces with a concomitant increase in the ICE, based on the consumption of current to forming a Li-Si alloy. Between 1.5 to 0.5 V vs. Li/Li⁺,^{42,43} decomposition of the electrolyte constituents leads to current consumption to generate a robust SEI; yet, at potentials below 0.2 V,⁴⁴ the formation of the Li-Si alloy initiates, and with lower potential limits, the capacity increase due to this formation leads to higher ICE.

Three-electrode full cells were then fabricated with pristine and pre-lithiated Li_{1+x}Mn₂O₄ powders as the cathode active material and Si/gr as the anode active material. Of note, Li_{2.0}MO was not tested due to its lowest ICE. All cells were designed with comparable charging capacities, as summarized in Table S4 and S5 of the electrode and cell specifications, and the calculated electrode performance is listed in Table S4 for the anode and Table S5 for the cathode. The discharge specific capacity of the cathodes (Li_{1+x}Mn₂O₄) increased by ~40% relative to pristine Li_{1.0}MO (Table 1). As a result, the specific discharge capacity from the Li_{1.0}MO is only 63 mAh g⁻¹ (Table 1) versus 105 mAh g⁻¹ capacity derived from half-cell tests. A key finding is that the actual discharge specific capacity of Li_{1.35}MO is 100 mAh g⁻¹, nearing the full discharge specific capacity obtained from half cells (102 mAh g⁻¹). Both cells exhibited comparable ICE since this parameter is dictated by the Si/gr anode, which has a lower or similar ICE as the cathode. As for the full cell comprising Li_{1.6}MO, the ICE is much lower than the cell with Li_{1.35}MO because of the lower ICE from Li_{1.6}MO (54% from half cells); thus, the Si/gr anode could not be fully lithiated/de-lithiated. Another important criterion is to understand the performance of these Si/gr||Li_{1+x}Mn₂O₄ cells to observe the voltage transients during charge/discharge (Fig. 3). For these cells, the Li_{1.0}MO potential stopped at 4.04 V vs. Li/Li⁺ at the end of discharge, while the potential was 3.86 V vs. Li/Li⁺ and 3.69 V vs. Li/Li⁺ for Li_{1.35}MO and Li_{1.6}MO, respectively, confirming that the pre-lithiated cathode materials have delivered higher reversible specific capacity than pristine Li_{1.0}MO.

Owing to the performance improvement of Li_{1.35}MO in a full-cell configuration, we carried out a more detailed investigation into the long-term stability for these cells (Fig. 4); expanded view of the discharge curves for the anode and cathode are shown in Fig. S3. Fig. 4 compares the cathode and anode potentials at two different cycle conditions (2nd vs. 30th cycle). We observed a potential shift in the anode and cathode potentials within these two conditions. The potential range was 0.15 V to 0.99 V for the anode and for the cathode, 3.90 V to 4.40 V in the 2nd cycle. After 30 cycles, the anode potential range shifted to 0.20 V to 0.98 V and for the cathode, 3.98 V to 4.45 V (Fig. 4a). The increase in the anode potential decreased the discharge capacity

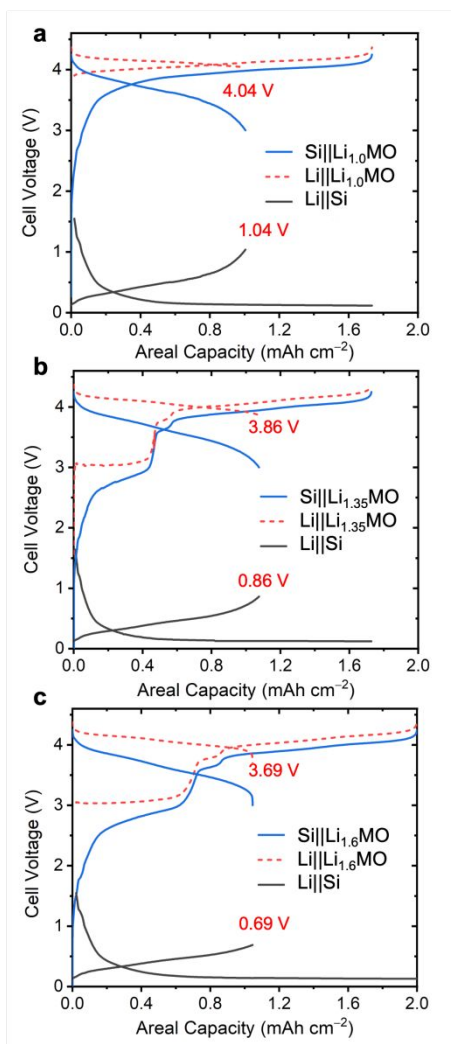


Fig. 3 First cycle charge/discharge curves using three-electrode full cells (lithium metal reference electrode) fabricated with (a) pristine $\text{Li}_{1.0}\text{MO}$, (b) pre-lithiated $\text{Li}_{1.35}\text{MO}$, and (c) pre-lithiated $\text{Li}_{1.6}\text{MO}$ as the cathode active materials and Si/gr as the anode active material. Charge and discharge operation were carried out at $C/5$ of the limiting electrode.

significantly (**Fig. 4b**; capacity loss of 30%) since the charging capability of the cathode was reduced, owing to the much shallower potential range. This was mainly attributed due to the resistance increase at the cathode. For the anode, the charging curve at the 30th cycle overlapped with the curve at the 2nd cycle with only a slight difference toward the end of charging, but the curve was much shorter. This suggests that the anode capacity loss is not the root cause for the cell capacity loss and the shallow potential range is the leading cause. To further improve cycle life, it will be essential to reduce the effect of the anode potential drift, which may require an efficient SEI formation process and a precisely controlled anode cycling potential range. It is also likely that optimizing the cell chemistry to tune the ICE of the Si anode during cycling will be beneficial.

In addition to the electrochemical performance of this series of pre-lithiated $\text{Li}_{1+x}\text{Mn}_2\text{O}_4$ electrodes, the ease of manufacturing must also be considered to handle these powders. Generally, with

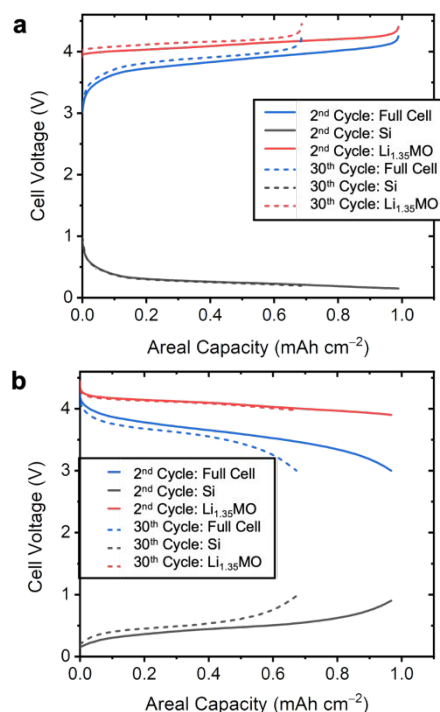


Fig. 4 Charge/discharge curves after the 2nd and 30th cycle of Si/gr|| $\text{Li}_{1.35}\text{MO}$ three-electrode cells during (a) charging of the full cell (charging of the cathode/discharging of the anode) and (b) discharging of the full cell (discharging of the cathode/charging of the anode).

pre-lithiated anode materials, these powders must be kept in an inert environment due to their sensitivity to moisture and oxygen; thus, they would create additional steps if integrated into current lithium-ion battery manufacturing. For this reason, we investigated the air stability of $\text{Li}_{1.35}\text{MO}$ by exposing the pre-lithiated powder to air (ambient conditions) for various durations (8 days and 30 days). No significant differences were observed, based on X-ray diffraction, of the powders before and after being ex-

posed to air (**Fig. S4**). After 30 days, a slight depression in the tetragonal phase was observed, suggesting that these powders' shelf-life under ambient conditions may need to be considered for long-term storage. The air-exposed $\text{Li}_{1.35}\text{MO}$ powders' stability was further tested in half-cell configurations to assess their performance over time. When the $\text{Li}_{1.35}\text{MO}$ powders are exposed to ambient conditions for one day, there is negligible capacity loss (**Table S6**). After eight days, the capacity loss is measured to be 86 mAh g^{-1} , decreasing by $\sim 16\%$, and after 30 days, the capacity remains the same. Of note, the ICEs remain comparable despite the exposure to air over time. Further investigation is needed to illustrate the relationship between the capacity change and the crystal structure change, particularly for the sample stored for eight days because the X-ray diffraction patterns did not reveal any structural change. The use of X-ray synchrotrons will be beneficial to probe deeper into the connection between structural change and moderate capacity loss, which will be the subject of future research.

In the present study, we demonstrate cursory prospects into

the air-stable pre-lithiated $\text{Li}_{1+x}\text{Mn}_2\text{O}_4$ cathode material that can be leveraged to properly tune lithiation content of the cathode material to balance the low Coulombic efficiencies of Si anode materials.

J.S.K., B.T., S.L., K.G. and M.W.L. acknowledge support from the Johns Hopkins University Applied Physics Laboratory (Independent Research and Development Funds) and the Office of Naval Research (N00024-13-D-6400).

Conflicts of interest

The authors declare no competing financial interest.

Notes and references

- 1 M. N. Obrovac and V. L. Chevrier, *Chemical reviews*, 2014, **114**, 11444–11502.
- 2 L. Sun, Y. Liu, R. Shao, J. Wu, R. Jiang and Z. Jin, *Energy Storage Materials*, 2022, **46**, 482–502.
- 3 K. Feng, M. Li, W. Liu, A. G. Kashkooli, X. Xiao, M. Cai and Z. Chen, *Small*, 2018, **14**, 1702737.
- 4 X. Zuo, J. Zhu, P. Müller-Buschbaum and Y.-J. Cheng, *Nano Energy*, 2017, **31**, 113–143.
- 5 Y. Liu, Y. Zhu and Y. Cui, *Nature Energy*, 2019, **4**, 540–550.
- 6 H. Andersen, C. Foss, J. Voje, R. Tronstad, T. Mokkelbost, P. Vullum, A. Ulvestad, M. Kirkengen and J. Mæhlen, *Silicon-Carbon composite anodes from industrial battery grade silicon*, *Sci. Rep.* 9 (2019) 1–9.
- 7 M. Jiang, J. Chen, Y. Zhang, N. Song, W. Jiang and J. Yang, *Advanced Science*, 2022, **9**, 2203162.
- 8 Y. Chabre and J. Pannetier, *Progress in Solid State Chemistry*, 1995, **23**, 1–130.
- 9 M. M. Thackeray, W. I. David, P. G. Bruce and J. B. Goodenough, *Materials research bulletin*, 1983, **18**, 461–472.
- 10 M. Thackeray, M. Mansuetto and J. Bates, *Journal of power sources*, 1997, **68**, 153–158.
- 11 Y. Ding, Z. P. Cano, A. Yu, J. Lu and Z. Chen, *Electrochemical Energy Reviews*, 2019, **2**, 1–28.
- 12 Z. Moorhead-Rosenberg, E. Allcorn and A. Manthiram, *Chemistry of Materials*, 2014, **26**, 5905–5913.
- 13 Y. Jin, B. Zhu, Z. Lu, N. Liu and J. Zhu, *Advanced Energy Materials*, 2017, **7**, 1700715.
- 14 L. Chen, C.-L. Chiang, X. Wu, Y. Tang, G. Zeng, S. Zhou, B. Zhang, H. Zhang, Y. Yan, T. Liu *et al.*, *Chemical Science*, 2023, **14**, 2183–2191.
- 15 F. Holtstiege, P. Bärmann, R. Nölle, M. Winter and T. Placke, *Batteries*, 2018, **4**, 4.
- 16 J. Ming, W. J. Kwak, S. J. Youn, H. Ming, J. Hassoun and Y.-K. Sun, *Energy Technology*, 2014, **2**, 778–785.
- 17 N. Liu, L. Hu, M. T. McDowell, A. Jackson and Y. Cui, *ACS nano*, 2011, **5**, 6487–6493.
- 18 C. L. Berhaut, D. Z. Dominguez, D. Tomasi, C. Vincens, C. Haon, Y. Reynier, W. Porcher, N. Boudet, N. Blanc, G. A. Chahine *et al.*, *Energy Storage Materials*, 2020, **29**, 190–197.
- 19 Y. Zhang, B. Wu, G. Mu, C. Ma, D. Mu and F. Wu, *Journal of Energy Chemistry*, 2022, **64**, 615–650.
- 20 J. Jang, I. Kang, J. Choi, H. Jeong, K.-W. Yi, J. Hong and M. Lee, *Angewandte Chemie International Edition*, 2020, **59**, 14473–14480.
- 21 T. Jia, G. Zhong, Y. Lv, N. Li, Y. Liu, X. Yu, J. Zou, Z. Chen, L. Peng, F. Kang *et al.*, *Green Energy & Environment*, 2023, **8**, 1325–1340.
- 22 C. L. Berhaut, D. Z. Dominguez, D. Tomasi, C. Vincens, C. Haon, Y. Reynier, W. Porcher, N. Boudet, N. Blanc, G. A. Chahine *et al.*, *Energy Storage Materials*, 2020, **29**, 190–197.
- 23 M. Marinaro, M. Weinberger and M. Wohlfahrt-Mehrens, *Electrochimica Acta*, 2016, **206**, 99–107.
- 24 V. Aravindan, S. Nan, M. Keppeler and S. Madhavi, *Electrochimica Acta*, 2016, **208**, 225–230.
- 25 D. Guyomard and J.-M. Tarascon, *Journal of the Electrochemical Society*, 1992, **139**, 937.
- 26 Z. Moorhead-Rosenberg, E. Allcorn and A. Manthiram, *Chemistry of Materials*, 2014, **26**, 5905–5913.
- 27 R. Zhan, X. Wang, Z. Chen, Z. W. Seh, L. Wang and Y. Sun, *Advanced Energy Materials*, 2021, **11**, 2101565.
- 28 C. Yang, H. Ma, R. Yuan, K. Wang, K. Liu, Y. Long, F. Xu, L. Li, H. Zhang, Y. Zhang *et al.*, *Nature Energy*, 2023, **8**, 703–713.
- 29 D. Peramunage and K. Abraham, *Journal of the Electrochemical Society*, 1998, **145**, 1131.
- 30 A. Mosbah, A. Verbaere and M. Tournoux, *Materials research bulletin*, 1983, **18**, 1375–1381.
- 31 Y. Shen, J. Zhang, Y. Pu, H. Wang, B. Wang, J. Qian, Y. Cao, F. Zhong, X. Ai and H. Yang, *ACS Energy Letters*, 2019, **4**, 1717–1724.
- 32 M. Cao, Z. Liu, X. Zhang, L. Yang, S. Xu, S. Weng, S. Zhang, X. Li, Y. Li, T. Liu *et al.*, *Advanced Functional Materials*, 2023, **33**, 2210032.
- 33 X. Liu, T. Liu, R. Wang, Z. Cai, W. Wang, Y. Yuan, R. Shahbazian-Yassar, X. Li, S. Wang, E. Hu *et al.*, *ACS Energy Letters*, 2020, **6**, 320–328.
- 34 A. Yamada and M. Tanaka, *Materials research bulletin*, 1995, **30**, 715–721.
- 35 J. B. Goodenough and K.-S. Park, *Journal of the American Chemical Society*, 2013, **135**, 1167–1176.
- 36 J. Zheng, R. Xia, S. Baiju, Z. Sun, P. Kaghazchi, J. E. Ten Elshof, G. Koster and M. Huijben, *ACS nano*, 2023, **17**, 25391–25404.
- 37 L. Xiao, Y. Guo, D. Qu, B. Deng, H. Liu and D. Tang, *Journal of Power Sources*, 2013, **225**, 286–292.
- 38 J. B. Goodenough and Y. Kim, *Chemistry of materials*, 2010, **22**, 587–603.
- 39 R. Jung, M. Metzger, D. Haering, S. Solchenbach, C. Marino, N. Tsiouvaras, C. Stinner and H. A. Gasteiger, *Journal of The Electrochemical Society*, 2016, **163**, A1705.
- 40 M. Wetjen, D. Pritzl, R. Jung, S. Solchenbach, R. Ghadimi and H. A. Gasteiger, *Journal of The Electrochemical Society*, 2017, **164**, A2840.
- 41 R. Petibon, V. Chevrier, C. Aiken, D. Hall, S. Hyatt, R. Shunmugasundaram and J. Dahn, *Journal of The Electrochemical Society*, 2016, **163**, A1146.
- 42 C. Cao, I. I. Abate, E. Sivonxay, B. Shyam, C. Jia, B. Moritz, T. P. Devereaux, K. A. Persson, H.-G. Steinrück and M. F. Toney, *Joule*, 2019, **3**, 762–781.
- 43 R. M. Kasse, N. R. Geise, J. S. Ko, J. N. Weker, H.-G. Steinrück and M. F. Toney, *Journal of materials chemistry A*, 2020, **8**, 16960–16972.
- 44 M. T. McDowell, S. W. Lee, W. D. Nix and Y. Cui, *Advanced materials*, 2013, **25**, 4966–4985.